Molecular and Cellular Neuroscience 128 (2024) 103916

Contents lists available at ScienceDirect

Molecular and Cellular Neuroscience

journal homepage: www.elsevier.com/locate/ymcne

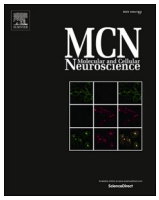

Amyloid-β deposits in human astrocytes contain truncated and highly resistant proteoforms

C. Beretta [a], E. Svensson [a,b], A. Dakhel [a], M. Zyśk [a], J. Hanrieder [c], D. Sehlin [a], W. Michno [a,d], A. Erlandsson [a,*]

[a] Department of Public Health and Caring Sciences, Molecular Geriatrics, Rudbeck Laboratory, Uppsala University, SE-752 37 Uppsala, Sweden
[b] Department of Neuroinflammation, UCL Queen Square Institute of Neurology, 1 Wakefield Street, WC1N 1PJ London, United Kingdom of Great Britain and Northern Ireland
[c] Department of Psychiatry and Neurochemistry, University of Gothenburg, SE-43180 Gothenburg, Sweden
[d] Science for Life Laboratory, Uppsala University, SE-752 37 Uppsala, Sweden

ARTICLE INFO

Keywords:
Alzheimer's disease
Amyloid β
Astrocytes
Aggregate

ABSTRACT

Alzheimer's disease (AD) is a neurodegenerative disorder that develops over decades. Glial cells, including astrocytes are tightly connected to the AD pathogenesis, but their impact on disease progression is still unclear. Our previous data show that astrocytes take up large amounts of aggregated amyloid-beta (Aβ) but are unable to successfully degrade the material, which is instead stored intracellularly. The aim of the present study was to analyze the astrocytic Aβ deposits composition in detail in order to understand their role in AD propagation. For this purpose, human induced pluripotent cell (hiPSC)-derived astrocytes were exposed to sonicated $Aβ_{42}$ fibrils and magnetic beads. Live cell imaging and immunocytochemistry confirmed that the ingested Aβ aggregates and beads were transported to the same lysosomal compartments in the perinuclear region, which allowed us to successfully isolate the Aβ deposits from the astrocytes. Using a battery of experimental techniques, including mass spectrometry, western blot, ELISA and electron microscopy we demonstrate that human astrocytes truncate and pack the Aβ aggregates in a way that makes them highly resistant. Moreover, the astrocytes release specifically truncated forms of Aβ via different routes and thereby expose neighboring cells to pathogenic proteins. Taken together, our study establishes a role for astrocytes in mediating Aβ pathology, which could be of relevance for identifying novel treatment targets for AD.

1. Introduction

Alzheimer's disease (AD) is characterized by the presence of amyloid plaques, neurofibrillary tangles, and chronic inflammation (Heneka et al., 2015; Serrano-Pozo et al., 2011). Although, these features were described already a century ago, the molecular and cellular mechanisms behind the pathology is still largely unknown. According to the amyloid cascade hypothesis, misfolding and aggregation of amyloid β (Aβ) is the driving force in AD progression (J. A. Hardy and Higgins, 1992; Hardy and Selkoe, 2002). A major concern with the amyloid cascade hypothesis is that the number of plaques does not correlate with the severity of dementia. However, emerging data, indicate that smaller, soluble Aβ aggregates, are more toxic than the insoluble fibrils and show better correlation with the severity of the symptoms (McLean et al., 1999; Näslund et al., 2000).

Astrocytes are the most abundant glial cell type in the brain and are crucial for maintaining brain homeostasis by supporting neurons and their synapses, as well as contributing to the blood brain barrier and the glymphatic system (Abbott et al., 2006; Allen, 2014; Hablitz et al., 2020; MacVicar and Newman, 2015; Mulica et al., 2021; Vasile et al., 2017). In the diseased brain, astrocytes acquire an inflammatory, reactive phenotype, but exactly how the AD pathology affects the astrocytes and their functions, and vice versa, it still not well understood (Olabarria et al., 2010; Pike et al., 1994). Reactive astrocytes are commonly found around Aβ plaques and have been shown to phagocytose both aggregated proteins and cellular debris (Koistinaho et al., 2004; Thal et al.,

* Corresponding author.
E-mail addresses: chiara.beretta@pubcare.uu.se (C. Beretta), elina.svensson.20@ucl.ac.uk (E. Svensson), abdulkhalek.dakhel@pubcare.uu.se (A. Dakhel), marlena.zysk@gumed.edu.pl (M. Zyśk), jorg.hanrieder@gu.se (J. Hanrieder), dag.sehlin@pubcare.uu.se (D. Sehlin), wojciech.michno@scilifelab.uu.se (W. Michno), anna.erlandsson@pubcare.uu.se (A. Erlandsson).

https://doi.org/10.1016/j.mcn.2024.103916
Received 27 October 2023; Received in revised form 8 January 2024; Accepted 15 January 2024
Available online 19 January 2024

2000). Our previous data demonstrate that astrocytes effectively take up large amounts of soluble Aβ aggregates. However, they are unable to successfully degrade the ingested material, which is instead accumulated as intracellular deposits (Konstantinidis et al., 2023a; Rostami et al., 2021; Söllvander et al., 2016). The Aβ-containing astrocytes are clearly stressed and show altered neuronal support and impaired mitochondrial dynamics. In addition, the Aβ-accumulation causes lysosomal dysfunction, resulting in enlarged endosomes and the release of extracellular vesicles (EVs) with extremely neurotoxic Aβ-content, which could be of relevance for AD progression (Beretta et al., 2020; Konstantinidis et al., 2023b; Zyśk et al., 2023). More specifically, EVs isolated from astrocytes treated with soluble Aβ aggregates induced synaptic loss, axonal swelling and vacuolization of the neuronal cell bodies, which consequently led to apoptosis of primary murine cortical neurons (Beretta et al., 2020). However, the exact properties of the astrocytic Aβ deposits and the reason why the secreted Aβ is extra harmful remain unclear. Hence, the aim of the present study was to uncover in which way astrocytes process and modify the ingested Aβ to make it more toxic.

2. Methods

2.1. Production of amyloid β fibrils

Amyloid-β preformed fibrils were generated using human $A\beta_{42}$ monomers (Innovagen, SP-BA42–1) and HiLyte™ Fluor 555-labeled $A\beta_{42}$ monomers (AnaSpec, 60480–01). The Aβ monomers were dissolved in a 10 mM NaOH/PBS solution to a concentration of 2 mg/ml. The Aβ samples were then left to aggregate on a shaker at 1500 rpm, 37 °C for 4 days. Prior to experiment, the $A\beta_{42}$ fibrils were diluted using peptide PBS to a concentration of 0.5 mg/ml and sonicated at 20 % amplitude, 1 s off and 1 s on, for 60 s using a Sonics Vibra Cell sonicator. For transmission electron microscopy (TEM), unsonicated or sonicated $A\beta_{42}$ fibrils were diluted 1:10 in Milli-Q water and dropped onto carbon coated 200-mesh copper grids, negatively stained with 2 % Uranyl acetate for 5 min and air dried. The samples were analyzed using a Tecnai G2 transmission electron microscope (FEI Company).

2.2. Culture of human iPSC derived astrocytes

Human astrocytes were generated from neuroepithelial-like stem (NES) cells, produced from human induced pluripotent stem cells (iPSCs, Cntrl9 cell line) (Falk et al., 2012; Lundin et al., 2018). The NES cells were plated at 60000 cells/cm^2 on 100 μg/ml poly-L-ornithine hydrobromide (#P3655, Merck, Darmstadt, Germany) and 4 μg/ml Laminin2020 (#L2020, Merck) double-coated culture vessels in Astrocyte differentiation medium; Advanced DMEM/F12 (ThermoFisher, 12634–010) supplemented with 1 % Penicillin Streptomycin (ThermoFisher, 15140–122), 1 % B27 supplement (ThermoFisher, 17504–044), 1 % non-essential amino acids (Merc Millipore) and 1 % L-Glutamine (ThermoFisher, 25030–024). The following factors were added fresh to the medium directly before use: 10 ng/ml basic fibroblast growth factor (bFGF) (ThermoFisher, 13256029), 10 ng/ml heregulin β-1 (Sigma-Aldrich, SRP3055), 10 ng/ml activin A (Peprotech, 120-14E) and 200 ng/ml insulin-like growth factor 1 (IGF-1) (Sigma-Aldrich, SRP3069). Additionally, 20 ng/ml ciliary neurotrophic factor (CNTF; ThermoFisher, PHC7015) was added to the medium during the last two weeks of differentiation. The medium was changed every other day and cells were passaged using Trypsin 0.05 % EDTA 0.2 g/l (Life Technologies) once the cells reached 80 % confluency. Directly after the 4 week differentiation period, the astrocytes were seeded for experiments at a concentration of 5000 cells/cm^2.

2.3. $A\beta_{42}$ and magnetic beads exposure

Astrocytes were exposed to 0.2 μM sonicated $A\beta_{42}$ fibrils and 10 μg/ml Dynabeads® MyOne™ Tosylactivated (Invitrogen, 65501) in astrocyte complete medium for 4 days. The concentration of Aβ was chosen based on our previous studies on human iPSC-derived astrocytes (Konstantinidis et al., 2023a; Konstantinidis et al., 2023b; Rostami et al., 2021; Zyśk et al., 2023). Control cultures received medium with 10 μg/ml magnetic beads alone. At day 4 the cells were washed two times with medium and were then cultured in $A\beta_{42}$-free medium. The cells were fixed or lysed at day 0, 7 or 14 following $A\beta_{42}$ fibril removal, i.e. 4d + 0d, 4d + 7d, and 4d + 14d. Conditioned medium was collected from the cultures at respective end point and stored at −80 °C.

2.4. Time-lapse microscopy

Time-lapse experiments were performed at 37 °C in 95 % O_2/5 % CO_2 using a Nikon Biostation IM Live Cell Recorder. Images were acquired at 20×, 40× and 80× magnifications every 10 min. The duration of the live imaging experiments were 72 h during the $A\beta_{42}$ fibril+magnetic bead exposure and 24 h for the later time points starting at day 0, 2, 7 and 14 post-treatment.

2.5. Immunocytochemistry

Cells were fixed with 4 % paraformaldehyde (PFA) (Sigma-Aldrich, P6148) in PBS for 15 min at RT and were then washed 3 times in PBS. Prior to antibody incubation, the cells were permeabilized and blocked in 0.1 % Triton X-100 in PBS with 5 % normal goat serum (NGS) (Bionordika, S-1000) for 30 min at RT. Primary antibodies (listed in Table 1) were diluted in 0.1 % Triton X-100 in PBS with 0.5 % NGS and added to the cells for 3 h at RT. The coverslips were then washed 3 times in PBS and incubated with secondary antibodies, diluted in 0.1 % Triton X-100 in PBS with 0.5 % NGS, for 45 min at 37 °C. The secondary antibodies used were AlexaFluor 488, 555 or 647 against mouse, rabbit or chicken (1:200, Molecular Probes). The coverslips were washed 3 times in PBS and mounted on microscope slides using EverBrite hard-set medium with DAPI (230032, Biotium). Images were captured using a fluorescence microscope Observer and Z1 Zeiss.

2.6. Cell lysis and magnetic precipitation of Aβ

The cells were lysed in ice-cold lysis buffer (20 mM Tris pH 7.5, 0.5 % Triton X-100, 0.5 % deoxycholic acid, 150 mM NaCl, 10 mM EDTA, 30 mM NaPyro), supplemented with a protease inhibitor cocktail (ThermoScientific). The lysates were transferred to protein LoBind tubes (Eppendorf) and incubated for 30 min on ice prior to centrifugation at 10000 xg for 10 min at 4 °C. A Dynabeads Magnetic Particle Concentrator (MPC-S; Applied Biosystems, A13346) was used to isolate the $A\beta_{42}$ and magnetic bead inclusions from the cell lysates. After isolation the beads were washed 3 times in PBS and incubated in 70 % formic acid +5 mM EDTA for one hour at 24°, vortexing every 15 min, to denature Aβ and separate it from the beads. After the formic acid treatment the samples were placed on the Dynabeads Magnetic Particle Concentrator for 2 min and the supernatant, containing the isolated Aβ, was collected and stored at −70 °C until analysis.

2.7. $A\beta_{42}$ ELISA

96-well EIA plates (Bio-Rad, 2240096) were coated with the C-terminus specific antibody anti-$A\beta_{42}$ (1 μg/ml; Table 1) in PBS overnight at 4 °C. Thereafter, the plates were blocked with 1 % bovine serum albumin (BSA) in PBS for 2 h at RT. Standard $A\beta_{42}$ monomers (American Peptide) were diluted in a 3.16× dilution series in ELISA incubation buffer (0.05 % Tween, 0.1 % BSA, 0.15 % Kathon in PBS at pH 7.4). Standard $A\beta_{42}$ (1 μg/ml) and samples were neutralised to pH 7 in 3 M Tris and diluted in a 10× dilution series in ELISA incubation buffer, to avoid impaired detection caused by aggregated Aβ and beads. Biotinylated mAb4G8 and 3D6 (Table 1), were used as secondary antibody

Table 1
Primary antibodies used.

Antibody	Host	Dilution	Target	Technique	Company	Cat #
Vimentin	Chicken	1:500	Astrocytes	ICC	Sigma Aldrich	AB5733
GLAST-1	Rabbit	1:400	Astrocytes	ICC	Novus Biologicals	NB100-1869
AQP4	Rabbit	1:200	Astrocytes	ICC	Novus Biologicals	NBP1-87679
GFAP	Chicken	1:400	Astrocytes	ICC	Abcam	ab4674
LAMP-1	Mouse	1:100	Lysosomes	ICC	Abcam	ab25630
S100β	Mouse	1:1000	Astrocytes	ICC	Sigma Aldrich	S2532
mAb4G8	Mouse	1:2000	Aβ		BioLegend	800705
3D6	Mouse	1:3000	Aβ N-terminal	WB, ELISA		custom production
Anti-$Aβ_{42}$	Rabbit	1:1000	Aβ C-terminal	WB, ELISA	Agrisera	custom production

and incubated for 1 h at RT, followed by incubation in streptavidin coupled horseradish peroxidase (ST-HRP; 1:2000; Mabtech, 3310–9-1000) for 1 h at RT. Thereafter, K-blue advanced (Neogen, 3119177) was used as HRP substrate with incubation for 15 min at RT, the reaction was stopped with 1 M H_2SO_4. Plates were measured at 450 nm in Tecan Infinity M200 PRO spectrophotometer (Tecan Group) and analyzed with Magellan v7.0 software (Tecan Group). Washing was performed between each step of the ELISA with 3 repetitions in washing buffer (phosphate buffered NaCl with 0.1 % Tween 20 and 0.15 % Kathon).

2.8. Isolation of extracellular vesicles

Conditioned culture medium from the different time points was pooled prior to ultracentrifugation. Then pooled medium samples for each treatment and cell culture batch were centrifuged at 300 ×*g* for 5 min to remove any free-floating cells, followed by another centrifugation at 2000 ×*g* for 10 min to remove any remaining cell debris. The supernatants were then collected and transferred to ultracentrifuge tubes and centrifuged at 135,000 ×*g* at 4 °C for 1.5 h to isolate EVs, including larger microvesicles and exosomes. The vesicle pellets were resuspended in 1 × PBS for TEM analysis or in ice-cold lysis buffer (20 mM Tris pH 7.5, 0.5 % Triton X-100, 0.5 % deoxycholic acid, 150 mM NaCl, 10 mM EDTA, 30 mM NaPyro), supplemented with a protease inhibitor cocktail (ThermoScientific, 78430) for analysis with Mass spectrometry.

2.9. Transmission electron microscopy of EVs and cells

2.9.1. EVs

EV samples were mixed with an equal volume of 4 % paraformaldehyde, added onto a formvar and carbon coated 200-mesh grid (Oxford 11 Instruments) and incubated for 20 min. After incubation, the grid was dried and washed first 3 times in PBS, followed by 8 washes in Milli-Q water. The samples were stained in a drop of Uranyl-oxalate, pH = 7, for 5 min, after which they were stained with a drop Uranyl-acetate 4 % pH = 4 with 2 % Methylcellulose on ice for 10 min. The dried grids were imaged in a Tecnai G2 transmission electron microscope (TEM, FEI company) with an ORIUS SC200 CCD camera and Gatan Digital Micrograph software (both from Gatan Inc.).

2.9.2. Cells

The cultures were fixed in 2.5 % glutaraldehyde and 1 % paraformaldehyde. The cells were then rinsed with 0.15 M sodium cacodylate (pH 7.2–7.4) for 10 min and incubated in fresh 1 % osmium tetraoxide in 0.1 M sodium cacodylate for 1 h at RT. After incubation, the sodium cacodylate was rinsed away to dehydrate the dishes with 70 % ethanol for 30 min, 95 % ethanol for 30 min and > 99 % ethanol for 1 h. A thin plastic layer (Agar 100 resin kit, Agar Scientific Ltd) was added to the dishes for 1 h. The plastic was then poured off and a new plastic layer was added onto the dishes for incubation overnight in a desiccator. Next, the plastic was heated to enable its removal after which a new thicker plastic layer was added before another incubation for 1 h in a desiccator. Cells were covered with 3 mm plastic and polymerized in the oven at 60 °C for 48 h. Embedded cells were sectioned by using a Leica ultracut UTC ultrotome (Rowaco AB) and visualized with a Tecnai G2 transmission electron microscope (FEI company) with an ORIUS SC200 CCD camera and Gatan Digital Micrograph software (both from Gatan Inc.).

2.10. Liquid chromatography mass spectrometry

N-terminally truncated Aβ peptides in the astrocyte cultures was verified through LC–MS/MS analysis as previously described, with few modifications (Michno et al., 2021). Briefly, the analysis with an alkaline mobile phase was carried out using a Q Exactive quadrupole–Orbitrap hybrid mass spectrometer equipped with a heated electrospray ionization source (HESI-II) (Thermo Scientific) and UltiMate 3000 binary pump, column oven, and autosampler (Thermo Scientific). The Q Exactive was operated in data-dependent mode. The resolution settings were 70.000 and target values were 1 × 106 both for MS and MS/MS acquisitions. Acquisitions were performed with 1 μscan/acquisition (Gkanatsiou et al., 2021; Michno et al., 2021). Precursor isolation width was 3 *m/z* units, and ions were fragmented using higher-energy collision-induced dissociation at a normalized collision energy of 25. Acquired LC–MS/MS data was processed using Xcalibur 2.2 Quanbrowser (Thermo Scientific). Spectra were deconvoluted using Mascot Distiller before submission to database search using the Mascot search engine (both Matrix Science) as described previously (Pannee et al., 2016). The MS/MS spectra were searched toward the SwissProt database containing the mutant human APP sequences using the following search parameters: taxonomy; *Homo sapiens*, precursor mass ± 15 ppm; fragment mass ± 0.05 Da; no enzyme; no fixed modifications; variable modifications including deamidated (NQ), Glu- > pyro-Glu (N-term E), oxidation (M); disulfide bonds (C—C) instrument default. Only peptides with ion score of around 100 were considered.

2.11. Western blot

Protein concentration was measured using BCA protein assay kit (Thermo Fisher Scientific, 23225) according to the manufacturer's protocol and a DeNovix DS-11 spectrophotometer using the A280 protein application for 4 kDa proteins. A total of 20 μg protein was mixed with Bolt LDS Sample buffer and Sample Reducing agent (Invitrogen, B0007) and incubated at 70 °C for 10 min. The samples were then loaded to a Bolt 4–12 % Bis-Tris gel (Invitrogen, NW04125BOX) together with a Chameleon Duo Pre-stained Protein Ladder (Li-Cor, 928–600000). The gel was run for 22 min at 200 V in Bolt MES SDS running buffer (Invitrogen, B0002) followed by transfer for 1 h at 10 V in Bolt transfer buffer (Invitrogen, BT00061) to a nitrocellulose membrane (Sigma-Aldrich, GE10600019) or PVDF membrane. The membrane was blocked in Odyssey blocking buffer (TBS) (Li-Cor, 927–50000) 1 h at RT and then incubated with the primary antibodies (Table 1) diluted in Odyssey blocking buffer (TBS) with 0.1 % Tween-20 (TBS-T) (1:1) overnight at 4 °C. Following 5 × 5 min washes in TBS-T, the membrane was incubated with the HRP-conjugated secondary antibodies goat anti-rabbit (1:10000; Sigma-Aldrich, A0545) and goat anti-mouse (1:10000;

Thermo Fisher Scientific, A16072) in Odyssey blocking buffer (TBS) with TBS-T (1:1) for 1 h at RT. Finally, the membrane was washed 5 × 5 min TBS-T, developed in enhanced chemiluminescence (ECL; GE Healthcare, RPN2232) and analyzed using the ChemiDoc XRS machine (Bio-Rad).

2.12. Statistical analysis

The Shapiro-Wilk normality test excluded normal distribution. Hence, the data was analyzed by one-way ANOVA with Kruskal-Wallis multiple comparison test, or nonparametric Mann Whitney test, using GraphPad Prism (version 5.03). For immunocytochemistry quantifications, 30 images per time point and treatment were captured at 40× magnification for each culture system. The IntDen fluorescence intensity signal and area was measured using ImageJ software. The ELISA and spectrophotometer graphs were based on $n = 3$, with an exception for Supplementary Fig. 3c. The results are shown as mean ± SD and the level of significance for all the graphs are: * = $P < 0.05$, ** = $P < 0.01$, *** = $P < 0.001$ and **** = $P < 0.0001$.

3. Results

3.1. Aβ and magnetic beads are stored in human astrocytes over a long time

Mature human iPSC-derived astrocytes, expressing the markers GLAST-1, vimentin, S100β, AQP4, GFAP (Supplementary Fig. 1a–e), were exposed to sonicated $Aβ_{42}$ fibrils and magnetic beads for 4 days, after which the cultures were thoroughly washed and cultured further in Aβ- and magnetic beads-free medium. The cells were then analyzed at 4d + 0d, 4d + 7d, 4d + 14d (Fig. 1a). Transmission electron microscopy (TEM) was performed as a quality check of the fibrils before and after sonication (Fig. 1b and c). In line with our previous data (Beretta et al., 2020; Konstantinidis et al., 2023a; Rostami et al., 2021; Söllvander et al., 2016), sonicated Aβ-fibrils were effectively engulfed by the human astrocytes and then stored intracellularly (Fig. 1d). Although, this Aβ accumulation could be stressful for the cells, there was no change in the number of live astrocytes during the experiment (Supplementary Fig. 1f).

To investigate if the Aβ and magnetic beads are simultaneously taken up by the astrocytes and stored together in the same cellular compartments, we followed the phagocytic process using time-lapse microscopy. By the end of the 4 days exposure period, the astrocytes had ingested large amounts of both Aβ and magnetic beads and over time, the internalized material was transported closer to the perinuclear region (Fig. 2a–b).

Live cell imaging of the phagocytic astrocytes for 14 days, confirmed that the ingested Aβ aggregates were not degraded, but rather stored and packed together, as we have previously shown (Rostami et al., 2021). This resulted in the formation of dense Aβ-bead inclusions around the nucleus (Fig. 2b). Taken together, these results verify that the Aβ and beads follow the same phagocytic route and accumulate together in the same organelles.

3.2. Stored Aβ and magnetic beads are situated in lysosomes

To further elucidate where the Aβ and magnetic beads are transported inside the astrocytes, we performed immunocytochemistry using the lysosomal marker LAMP-1 at 4d + 0d, 4d + 7d and 4d + 14d. At all three time points the engulfed Aβ and magnetic beads were found close to LAMP-1+ areas (Fig. 3a), indicating that at least part of the material enters the lysosomes. Over time, the size of LAMP-1+ lysosomes increased (Fig. 3b), suggesting an activation of the lysosomal degradation pathway. Confocal imaging revealed that both Aβ and magnetic

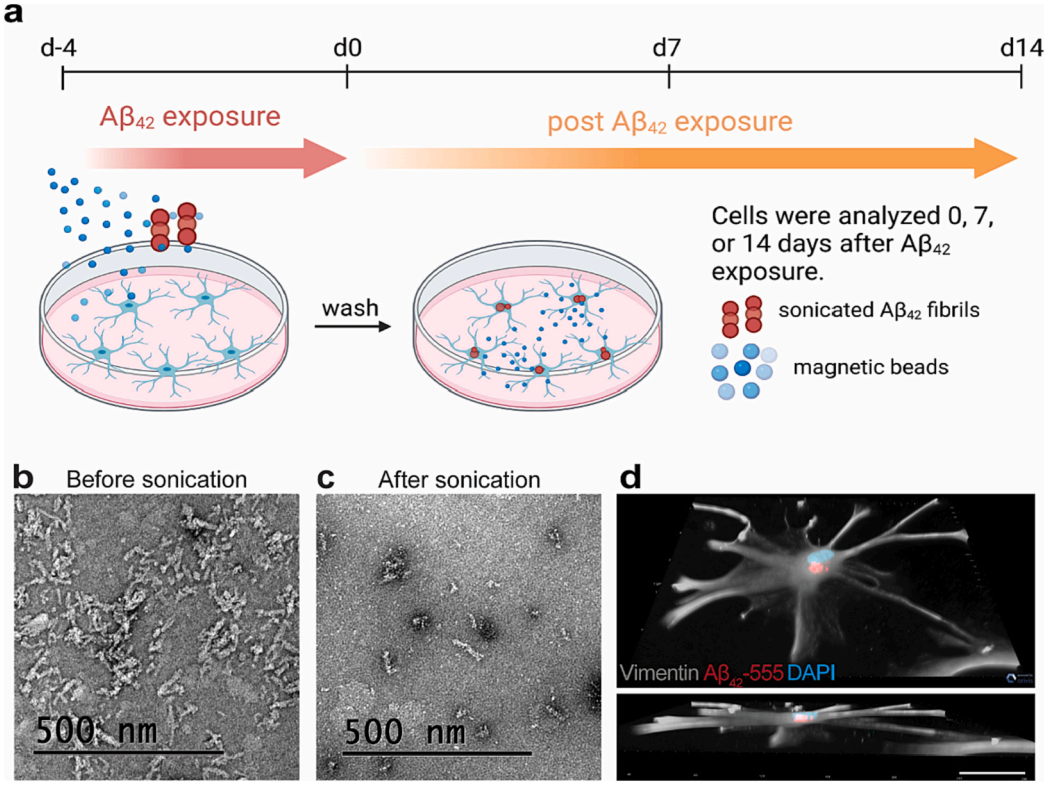

Fig. 1. Model to study Aβ-pathology in human astrocytes. Human iPSC-derived astrocytes were exposed to sonicated $Aβ_{42}$ fibrils and magnetic beads for 4 days after which the cultures were washed and maintained in Aβ-free medium for 0, 4 and 14 days prior to analysis, i.e. 4d + 0d, 4d + 7d, and 4d + 14d (a). Representative transmission electron microscopy images of Aβ fibrils before (b) and after sonication (c). 3D rendering of an astrocyte with intracellular Aβ-inclusions from two different angles (d). Scale bar (d): 40 μm.

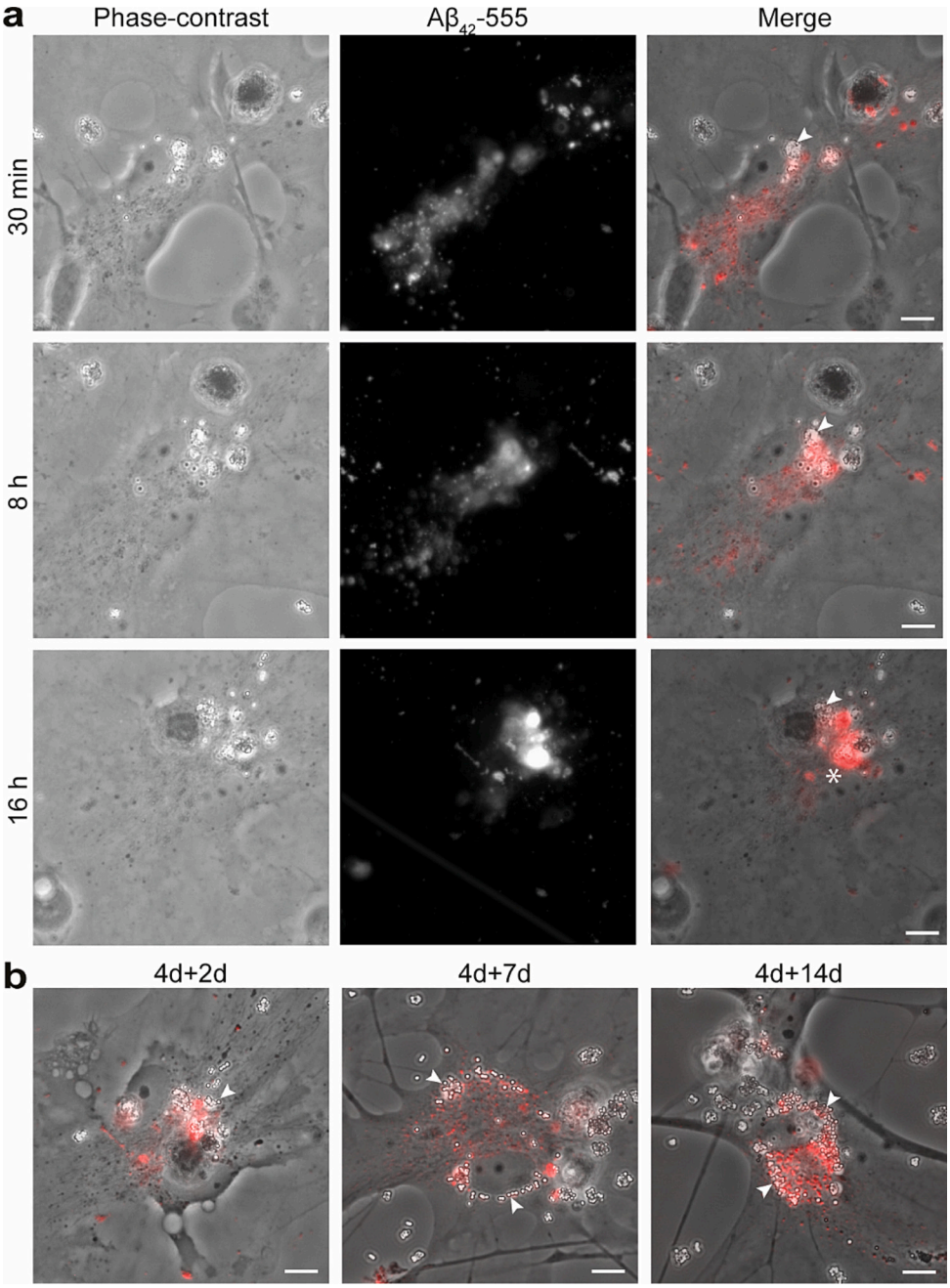

Fig. 2. Ingested $A\beta_{42}$-aggregates accumulate together with magnetic beads in human astrocytes. Live cell imaging of astrocytes after the 4 days exposure, demonstrated a continuous accumulation and trafficking of $A\beta_{42}$-fibrils and magnetic beads (white arrowheads), resulting in formation of dense inclusions at 16 h (white asterisk, a). Time-lapse images from 4d + 2d, 4d + 7d, and 4d + 14d showed an increased intracellular aggregation and concentration of Aβ and magnetic beads around the nuclei over time (b). Scale bars: 10 μm.

beads were surrounded by LAMP-1 at 4d + 14d (Fig. 3c–c′). Interestingly, the co-localization between LAMP-1 and Aβ were increased at both 4d + 7d and 4d + 14d, compared to 4d + 0d, suggesting an accumulation of Aβ in the lysosomes over time (Fig. 3d). Moreover, electron microscopy confirmed the presence of the magnetic beads inside lysosomal vesicles in the astrocytes (Fig. 3e, Supplementary Fig. 2).

3.3. *Phagocytic astrocytes produce truncated Aβ species*

To investigate how the intracellular storage affected the Aβ-aggregates, we next sought to isolate the astrocytic 555-Aβ and beads-inclusions (Supplementary Fig. 3a). To optimize the extraction method, we first compared cell homogenization using lysis buffer and mechanical homogenization through scraping and pipetting. Microscopy images showed that the beads were surrounded by Aβ-555 fibrils in both cases (Supplementary Fig. 3b). However, ELISA analysis of the extracted Aβ indicated a higher yield of Aβ following isolation through homogenization with lysis buffer (Supplementary Fig. 3c). Hence, we choose to use this method throughout the study. Next, we treated the beads/Aβ-isolates with formic acid to denature Aβ and removed the beads using a Dynabeads Magnetic Particle Concentrator.

To study the composition of the intracellularly stored aggregates over time, Aβ isolated from astrocytes at day 0, 7 and 14 post-exposure, was analyzed with sandwich ELISA. Two different primary antibodies were used; 4G8 and 3D6. The 4G8 antibody is specific for the mid-region of the $A\beta_{42}$ peptide, therefore capturing both full-length and truncated

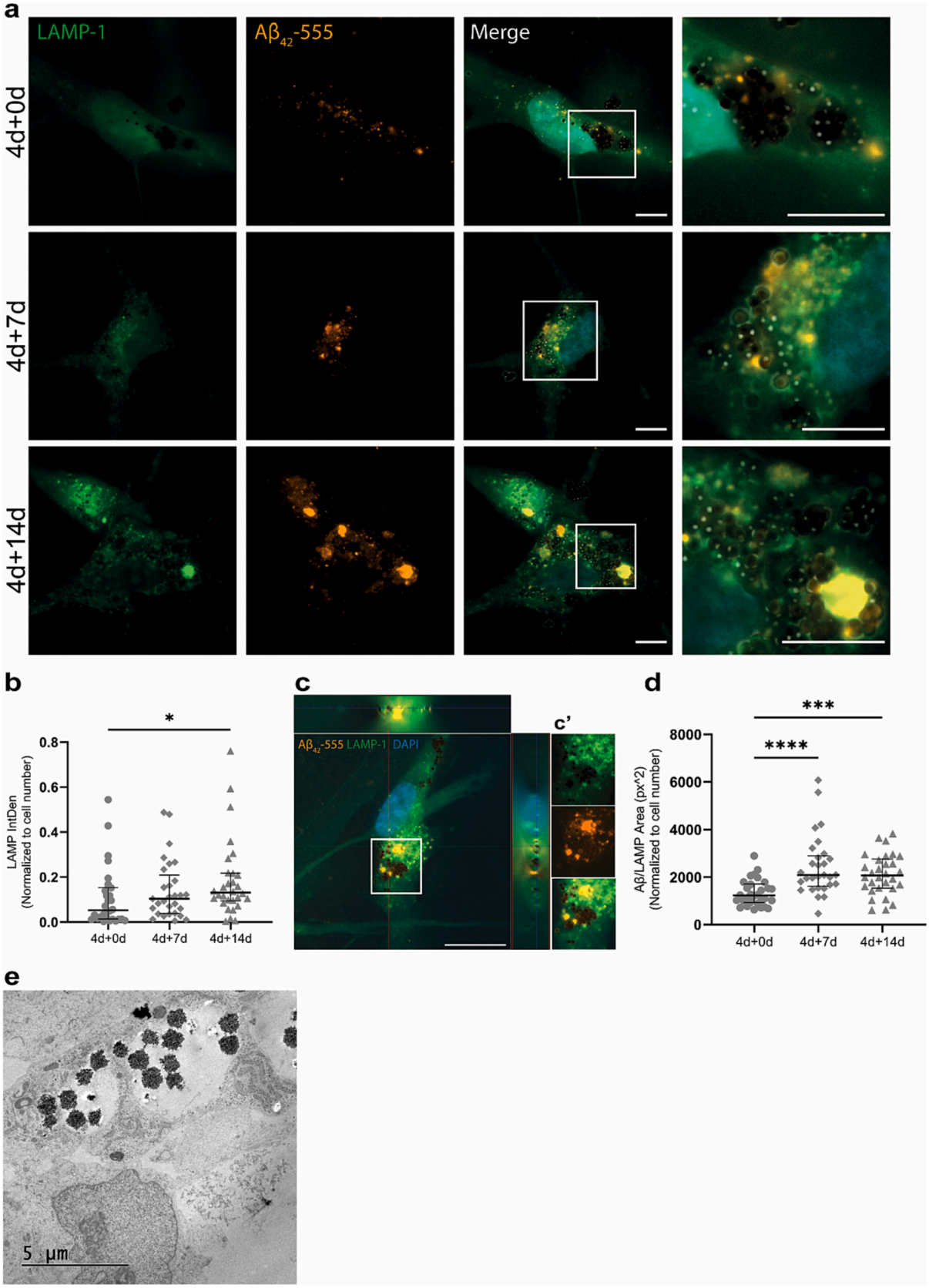

Fig. 3. Intracellular stored Aβ and magnetic beads are found in LAMP-1+ compartments. Immunocytochemistry of astrocytes indicated that Aβ-555 and magnetic beads were located in LAMP-1+ organelles, that increased in size over time (a). Quantification of the LAMP1 signal, confirmed an increased intensity at the latest time point (b). Confocal microscopy verified the presence of magnetic beads and Aβ in LAMP-1 + organelles at 4d + 14d (c–c′). The area of co-localization between LAMP1 and Aβ-555 showed a significant increase at the two latest time points, compared to 4d + 0d (d).Electron microscopy displayed the presence of magnetic beads inside degradation organelles (e). Scale bars: 10 μm.

Aβ species, while 3D6 binds to the N-terminal of Aβ and therefore give no signal if the Aβ is N-truncated. The ratio between 3D6 and 4G8 indicated an increase in N-truncation over time in Aβ isolated from the astrocytes, compared to control Aβ fibrils (Fig. 4a), implying an incomplete lysosomal degradation, which is in line with our previous results (Söllvander et al., 2016). No Aβ was detected in the isolates from the control astrocytes. To further investigate how astrocytes modify the stored Aβ, we performed liquid chromatography mass spectrometry (LC-MS/MS) analysis of the conditioned media, cell lysates, and extracellular vesicles (EVs) secreted from the astrocytes (Fig. 4b-c). While the conditioned medium was analyzed directly, the EVs were isolated by ultracentrifugation from a larger volume of conditioned medium, followed by treatment with lysis buffer to expose the EV content. Hence, analysis of the conditioned medium reveals the forms of Aβ that is free-floating in the medium, while the EV analysis reveals the forms of Aβ that are localized inside the EVs. Using this approach, we were able to identify multiple C-terminally truncated peptides in the conditioned medium, including Aβ1–40, Aβ1–39, Aβ1–38, as well as a few N-terminally truncated forms of the Aβx-40 peptide. Interestingly, a different peptide pattern was present in the extract from cells and from the extracellular vesicles. In the cell lysates we detected N-terminally truncated forms of the Aβx-42 peptide. These were specifically truncated before serine at position 26 in the Aβ sequence (Aβ26–42), and phenylalanine at position 19 (Aβ19–42). Extracellular vesicles contained the same peptides, with a few additional truncation of the Aβx-42 peptide at either glutamic acid 3 (Aβ3–42), glycine 25 (Aβ25–42), or lysine (Aβ28–42). Here we also observed the Aβ1–40 species. Overall, this supports the ELISA data indicating that astrocyte do indeed process Aβ internally at the N-terminus. Additionally the data suggests the presence of at least two different pools of Aβ that comes from astrocytes, including N-terminally truncated peptides, likely actively secreted through vesicular transport, and C-terminally peptides that are passively released into the media.

3.4. *Highly resistant Aβ proteoforms increases over time in phagocytic astrocytes*

To further evaluate the concentration of the isolated Aβ, we took advantage of the Fluor 555 tag on the Aβ fibrils and quantified the fluorescent signal using a DeNovix DS-11 spectrophotometer. This showed a significant increase in the concentration of $Aβ_{42}$ in the isolated intracellular inclusions over time (Fig. 5a), which could be explained by the fact that Aβ and magnetic beads are brought closer together over time. Following ingestion, protein aggregates are relocated inside the cell to end up in "storage dumps" (in this case together with the beads), a phenomenon that we have previously documented using different astrocytic culture systems after astrocytic engulfment of Aβ, α-syn or tau aggregates (Konstantinidis et al., 2023a; Konstantinidis et al., 2023b; Lindström et al., 2017; Mothes et al., 2023; Rostami et al., 2017, 2021; Söllvander et al., 2016; Streubel-Gallasch et al., 2021; Zyśk et al., 2023). Moreover, western blot analysis using the C-terminal specific Anti-$Aβ_{42}$ antibody (Fig. 5b, Supplementary Fig. 4a–c), and the N-terminal specific 3D6 antibody (Fig. 5c, Supplementary Fig. 4b) verified that the intracellular Aβ was partially truncated. Interestingly the isolated Aβ appeared at a molecular weight around 55 kDa and the concentration of this proteoform increased over time, confirming our DeNovix DS-11 spectrophotometer data. This suggests that the astrocytes process the accumulated Aβ to form stable protein proteoforms. These aggregates are not denatured after formic acid treatment, meaning that they are highly resistant to even harsh denaturing steps, while smaller oligomers is most likely broken down during the process. To further investigate how the astrocytes modify the intracellularly stored Aβ, we performed electron microscopy on the isolated Aβ following sonication (Fig. 5d). Interestingly, the astrocyte-isolated Aβ was more resistant to sonication and had a very different appearance compared to control fibrils (Fig. 5d–e). This data indicates that astrocytes pack the stored Aβ in a way that makes it more stable and changes its morphology.

4. Discussion

Growing evidence indicates that glial cells, including astrocytes are tightly connected to AD pathogenesis (Ding et al., 2021). Astrocytes are highly phagocytic and have been shown to engulf both dead cells and various amyloid proteins, including Aβ (Damisah et al., 2020; Domínguez-Prieto et al., 2018; Lööv et al., 2015; Morizawa et al., 2017). While astrocytes effectively degrade monomeric Aβ-peptides(Basak et al., 2012; Koistinaho et al., 2004; Söllvander et al., 2016), aggregated Aβ forms are not processed in the same manner. Although, the astrocytes take up very large amounts of the Aβ aggregates, they seem to be overwhelmed by the difficulties they face and are unable to fully degrade the protein. Instead, of being digested, the Aβ aggregates are shuffled around intracellularly and end up as large inclusions that are not easily cleared (Nielsen et al., 2010; Söllvander et al., 2016). In a recent study we demonstrated that after 10 weeks of culturing (in Aβ-free medium), hiPSC-derived astrocytes retain the ingested Aβ-deposits, indicating that astrocytes store Aβ aggregates for a very long time (Konstantinidis et al., 2023a). Importantly, astrocytic inclusions of Aβ have been reported to be present in the cortex of post mortem human AD brains and their size correlates with the pathology in the respective region (Nagele et al., 2003; Thal et al., 2000). We hypothesized that the

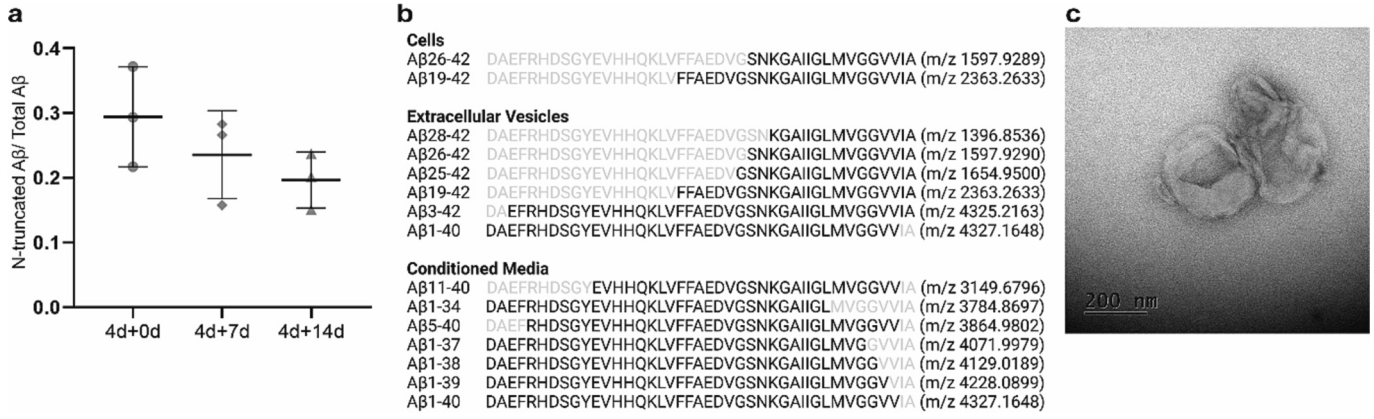

Fig. 4. Increased N-truncation of Aβ in human astrocytes over time. The ratio of Aβ detected with the N-terminal specific antibody 3D6 and the mid-region binding antibody 4G8 shows an increase of N-truncation over time from 0 to 14 days after the Aβ exposure (a). LC-MS analysis identified C-truncated Aβ in the astrocytic conditioned media, while the Aβ found in the cell lysates and EV fraction was mainly N-truncated (b). TEM confirmed the presence of EVs secreted from the astrocytes (c).

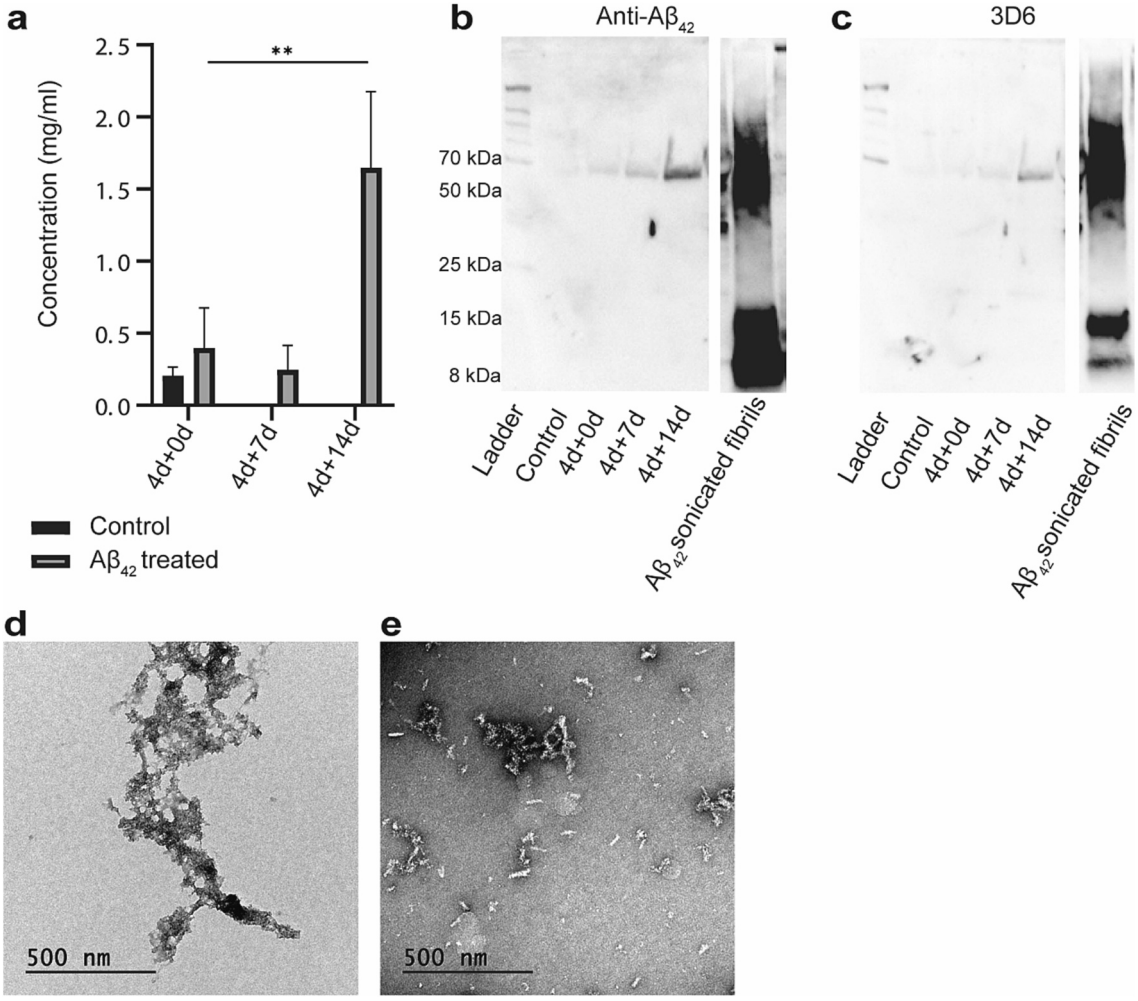

Fig. 5. Aβ concentration in isolated samples from astrocytes increase over time. DeNovix DS-11 spectrophotometer measurements of Aβ concentration demonstrated a significant increase of intracellular Aβ over time (4d + 0d: 0.40 ± 0.28, 4d + 14d) (a). Western blot analysis of isolated Aβ inclusions confirmed an increased concentration over time. Aβ was detected with both the C-terminal specific antibody anti-$Aβ_{42}$ (Agrisera) (b) and the N-terminal specific antibody 3D6 (c). Control samples were obtained from cells exposed to magnetic beads only (4 + 0 days). Sonicated control $Aβ_{42}$ fibrils were also included in the analysis. TEM imaging of sonicated Aβ aggregates isolated from human astrocytes showed a denser morphology (d) compared to sonicated control $Aβ_{42}$ fibrils (e).

long-term storage by astrocytes may affect the Aβ properties. Hence, the aim of this study was to investigate how hiPSC-derived astrocytes process and modify the intracellular Aβ.

To isolate the astrocytic Aβ deposits we used superparamagnetic dynabeads, which bind to the $Aβ_{42}$ primary amine groups via their p-toluene-sulfonyl groups. Our immunocytochemistry data clearly showed that both the Aβ aggregates and the beads were effectively internalized by the human astrocytes. Over time, the ingested material was transported toward the centre of the cell and packed together in dense inclusions in the perinuclear region. We and others have reported that astrocytic Aβ-inclusions co-localize with LAMP-1-positive organelles, suggesting a direct impact of lysosomes in the storage and degradation of Aβ-aggregates (Basak et al., 2012; Konstantinidis et al., 2023a; Söllvander et al., 2016). Consistent with those reports, we found that the bead+Aβ inclusions were situated in LAMP-1+ compartments. Moreover, electron microscopy analysis confirmed the presence of the magnetic beads within lysosomal/endosomal vesicles in the astrocytes.

Mutations in APP are known to result in familial AD by increasing the Aβ levels (Andrade-Guerrero et al., 2023). However, patients with sporadic AD, which accounts for over 95 % of the cases, do not have an increased Aβ production. Instead, the main cause of this form of the disease is believed to be insufficient Aβ clearance by the lysosomal machinery (Nixon, 2020). The ELISA based ratio between 3D6 and 4G8 signal in this study indicates that a large proportion of the Aβ in the astrocytic deposits is N-truncated. As we exposed the astrocytes to full-length $Aβ_{42}$ aggregates, we could conclude that the truncation of Aβ occurs in the lysosomes/endosomes. Importantly, truncated Aβ has been shown to be more resistant to degradation, more prone to aggregate, have a higher seeding capacity and more toxic than full length Aβ (De Kimpe et al., 2013). We have previously reported that Aβ-containing murine astrocytes release EVs with neurotoxic Aβ-content (Söllvander et al., 2016). Interestingly, we detected a significant increase in apoptotic, TUNEL+ neurons in cultures treated with EVs from Aβ42 protofibril exposed astrocytes. However, parallel neuronal cultures, exposed to intact Aβ42 protofibrils, directly added to the medium, showed no difference in the percentage of apoptotic cells, compared to untreated cultures (Söllvander et al., 2016). Hence, our data indicate that the truncated Aβ-aggregates that have been modified by astrocytes are more toxic than full-length aggregates.

Astrocytes are considered to be the major secretory cells in the brain, responsible for the release of neurotransmitters, growth factors, inflammatory mediators, and toxic proteins (Verkhratsky et al., 2016). Our previous investigations show that incomplete degradation of Aβ by astrocytes causes secretion of EVs, containing truncated, neurotoxic Aβ species and increased levels of apoE (Beretta et al., 2020; Nikitidou et al., 2017; Rostami et al., 2021; Söllvander et al., 2016). Here, we used

LC-MS/MS analysis to fully characterize the truncation pattern of Aβ peptides secreted into the medium via passive release or via EVs. Interestingly we noticed that the Aβ was secreted differently depending on the type of truncation. Aβ found in the conditioned medium (passive release) was C-terminal truncated, while the Aβ in the EV-fraction (active release) was mainly N-truncated. More specifically, we found multiple C-terminally truncated peptides in the conditioned medium, including Aβ1–40, Aβ1–39, Aβ1–38, as well as few N-terminally truncated forms of the Aβx-40 peptide. In the EV-fraction, the pattern was completely different, consisting mainly of N-terminally truncated forms of the Aβx-42 peptide, such as Aβ26–42Aβ19–42, Aβ3–42, Aβ25–42 and Aβ28–42. We also performed LC-MS/MS analysis of cell lysates. The intracellular Aβ-deposits contained N-terminally truncated forms of the Aβx-42 peptide, which highly overlapped with the EV-fraction. These findings suggest that there are at least two different pools of Aβ, including N-terminally truncated peptides that are actively secreted through vesicular transport, and C-terminally peptides that are passively released directly into the media. Due to the different secretion routes, we speculated that the C-terminally truncated Aβ might arise from an endogenous Aβ production by the stressed astrocytes, while the N-truncated Aβ most likely are generated from the externally added Aβ aggregates that are ingested by the astrocytes and accumulated in the lysosomes. In line with our findings, both N- and C-terminal truncated Aβ has been found in the human AD brain (Wildburger et al., 2017).

Western blot analysis revealed a distinct 55 kDa Aβ proteoform in the astrocyte-deposits that increased in concentration with time. The 55 kDa Aβ aggregates were highly SDS resistant and could not be denatured by formic acid treatment. Moreover, electron microscopy of the astrocytic Aβ deposits displayed a very different morphology compared to in vitro-aggregated fibres. Notably, the astrocytic Aβ aggregates did not show a typical fibrillary structure. In addition, the astrocytic Aβ deposits were remarkably resistant to sonication. Taken together, these results indicate that astrocytes process intracellularly stored Aβ so it becomes much more stable. This finding is supported by Bouter et al. who observed that N-terminal truncated Aβ (Aβ4–40 and AβpE3–42) are more aggregation-prone than full length Aβ1–42 and form stable aggregates over time that do not show a typical fibrillary structure (similar to our EM images) (Bouter et al., 2013). However, in contract to the distinct 55 kDa Aβ aggregate isolated from the astrocytes in our study, Bouter et al. reports a range of aggregates of higher molecular weight. However, it is important to note that these samples were not formic acid-treated.

Interestingly, we have noticed that protein aggregates in the human astrocytes can be difficult to detect with commercially available antibodies. Presumably, because the astrocytes have modified the proteins in a way so that the antibodies do not recognize them any longer. Most of the N-terminal truncations we found are extensive and it is possible that the cells have modified the aggregates also in other ways. By staining human brain sections with antibodies that bind to astrocyte-modified Aβ, we might get a completely new view of the pathology.

Although AD is the leading cause of dementia there are no treatment available that effectively limits the neurodegeneration and slows down the disease progression. Hence, a better understanding of the cellular and molecular mechanisms of the disease is highly desirable. Here we show that astrocytes may serve as an intermediator, promoting spreading of Aβ species with enhanced pathological properties. Following ingestion, the astrocytes process, pack and truncate the Aβ aggregates in a way that makes them highly resistant. Moreover, the astrocytes release modified Aβ species via direct secretion and via EVs and thereby expose neighboring cells to pathogenic proteins. In conclusion, our data highlight the importance of astrocytes in Aβ-mediated pathology, suggesting that this cell type may be a potent treatment target.

Funding

This study was supported by grants from the Swedish Research Council (2021-02563), the Swedish Alzheimer Foundation (AF-980656), Åhlén Foundation (223037), the Swedish Brain Foundation (FO2022-0083), Stiftelsen för Gamla Tjänarinnor (2021-01171), O. E. och Edla Johanssons Vetenskapliga Stiftelse (2021), Stiftelsen Olle Engkvist Byggmästare (215-0399), Bertil and Ebon Norlin Foundation and Stohnes Stiftelse (2021).

Ethical approval and consent to participate

The Cntrl9 hiPSC line was originally established from a human dermal biopsy of a healthy individual by the iPS Core Facility at Karolinska Institutet, following approval by the Ethics Review Board in Stockholm (registration number: 2012/208–31/3) and patient consent.

Consent for publication

Not applicable.

CRediT authorship contribution statement

C. Beretta: Conceptualization, Data curation, Formal analysis, Funding acquisition, Investigation, Methodology, Project administration, Validation, Writing – original draft, Writing – review & editing. **E. Svensson:** Conceptualization, Data curation, Formal analysis, Investigation, Methodology, Validation, Visualization, Writing – original draft. **A. Dakhel:** Methodology, Visualization, Writing – original draft, Writing – review & editing. **M. Zyśk:** Methodology, Visualization, Writing – original draft. **J. Hanrieder:** Validation, Visualization, Writing – original draft. **D. Sehlin:** Validation, Visualization, Writing – original draft. **W. Michno:** Methodology, Validation, Visualization, Writing – original draft, Writing – review & editing. **A. Erlandsson:** Data curation, Formal analysis, Funding acquisition, Investigation, Methodology, Project administration, Resources, Supervision, Validation, Visualization, Writing – original draft, Writing – review & editing.

Declaration of competing interest

The authors declare that they have no competing interest.

Availability of data and materials

The datasets used and/or analyzed during the current study are available from the corresponding author on reasonable request.

Acknowledgements

We thank Monika Hodik and Karin Staxäng at the BioVis core facility, Uppsala University, for technical assistance with TEM.

Graphical abstract, Figs. 1a, and 4d were created with BioRender.com.

Appendix A. Supplementary data

Supplementary data to this article can be found online at https://doi.org/10.1016/j.mcn.2024.103916.

References

Abbott, N.J., Rönnbäck, L., Hansson, E., 2006. Astrocyte–endothelial interactions at the blood–brain barrier. Nat. Rev. Neurosci. 7 (1), 41–53. https://doi.org/10.1038/nrn1824.

Allen, N.J., 2014. Astrocyte regulation of synaptic behavior. Annu. Rev. Cell Dev. Biol. 30 (1), 439–463. https://doi.org/10.1146/annurev-cellbio-100913-013053.

Andrade-Guerrero, J., Santiago-Balmaseda, A., Jeronimo-Aguilar, P., Vargas-Rodríguez, I., Cadena-Suárez, A.R., Sánchez-Garibay, C., Pozo-Molina, G., Méndez-Catalá, C.F., Cardenas-Aguayo, M.-D.-C., Diaz-Cintra, S., Pacheco-Herrero, M., Luna-Muñoz, J., Soto-Rojas, L.O., 2023. Alzheimer's disease: an updated overview of its genetics. Int. J. Mol. Sci. 24 (4), 3754. https://doi.org/10.3390/ijms24043754.

Basak, J.M., Verghese, P.B., Yoon, H., Kim, J., Holtzman, D.M., 2012. Low-density lipoprotein receptor represents an apolipoprotein E-independent pathway of Aβ uptake and degradation by astrocytes. J. Biol. Chem. 287 (17), 13959–13971. https://doi.org/10.1074/JBC.M111.288746.

Beretta, C., Nikitidou, E., Streubel-Gallasch, L., Ingelsson, M., Sehlin, D., Erlandsson, A., 2020. Extracellular vesicles from amyloid-β exposed cell cultures induce severe dysfunction in cortical neurons. Sci. Rep. 10 (1), 1–14. https://doi.org/10.1038/s41598-020-72355-2.

Bouter, Y., Dietrich, K., Wittnam, J.L., Rezaei-Ghaleh, N., Pillot, T., Papot-Couturier, S., Lefebvre, T., Sprenger, F., Wirths, O., Zweckstetter, M., Bayer, T.A., 2013. N-truncated amyloid β (Aβ) 4-42 forms stable aggregates and induces acute and long-lasting behavioral deficits. Acta Neuropathol. 126 (2), 189–205. https://doi.org/10.1007/s00401-013-1129-2.

Damisah, E.C., Hill, R.A., Rai, A., Chen, F., Rothlin, C.V., Ghosh, S., Grutzendler, J., 2020. Astrocytes and microglia play orchestrated roles and respect phagocytic territories during neuronal corpse removal in vivo. Science. Advances 6 (26), eaba3239. https://doi.org/10.1126/sciadv.aba3239.

De Kimpe, L., van Haastert, E.S., Kaminari, A., Zwart, R., Rutjes, H., Hoozemans, J.J.M., Scheper, W., 2013. Intracellular accumulation of aggregated pyroglutamate amyloid beta: convergence of aging and Aβ pathology at the lysosome. Age 35 (3), 673–687. https://doi.org/10.1007/s11357-012-9403-0.

Ding, Z. Bin, Song, L.J., Wang, Q., Kumar, G., Yan, Y.Q., Ma, C.G., 2021. Astrocytes: a double-edged sword in neurodegenerative diseases. Neural Regen. Res. 16 (9), 1702–1710. https://doi.org/10.4103/1673-5374.306064.

Domínguez-Prieto, M., Velasco, A., Tabernero, A., Medina, J.M., 2018. Endocytosis and transcytosis of amyloid-β peptides by astrocytes: a possible mechanism for amyloid-β clearance in Alzheimer's disease. Journal of Alzheimer's Disease: JAD 65 (4), 1109–1124. https://doi.org/10.3233/JAD-180332.

Falk, A., Koch, P., Kesavan, J., Takashima, Y., Ladewig, J., Alexander, M., Wiskow, O., Tailor, J., Trotter, M., Pollard, S., Smith, A., Brüstle, O., 2012. Capture of neuroepithelial-like stem cells from pluripotent stem cells provides a versatile system for in vitro production of human neurons. PLoS One 7 (1), e29597. https://doi.org/10.1371/journal.pone.0029597.

Gkanatsiou, E., Sahlin, C., Portelius, E., Johannesson, M., Söderberg, L., Fälting, J., Basun, H., Möller, C., Odergren, T., Zetterberg, H., Blennow, K., Lannfelt, L., Brinkmalm, G., 2021. Characterization of monomeric and soluble aggregated Aβ in Down's syndrome and Alzheimer's disease brains. Neurosci. Lett. 754, 135894 https://doi.org/10.1016/j.neulet.2021.135894.

Hablitz, L.M., Plá, V., Giannetto, M., Vinitsky, H.S., Stæger, F.F., Metcalfe, T., Nguyen, R., Benrais, A., Nedergaard, M., 2020. Circadian control of brain glymphatic and lymphatic fluid flow. Nat. Commun. 11 (1), 4411. https://doi.org/10.1038/s41467-020-18115-2.

Hardy, J.A., Higgins, G.A., 1992. Alzheimer's disease: the amyloid cascade hypothesis. Science (New York, N.Y.) 256 (5054), 184–185. https://doi.org/10.1126/science.1566067.

Hardy, J., Selkoe, D.J., 2002. The amyloid hypothesis of Alzheimer's disease: progress and problems on the road to therapeutics. Science 297 (5580), 353–356. https://doi.org/10.1126/science.1072994.

Heneka, M.T., Carson, M.J., El Khoury, J., Landreth, G.E., Brosseron, F., Feinstein, D.L., Jacobs, A.H., Wyss-Coray, T., Vitorica, J., Ransohoff, R.M., Herrup, K., Frautschy, S. A., Finsen, B., Brown, G.C., Verkhratsky, A., Yamanaka, K., Koistinaho, J., Latz, E., Halle, A., Kummer, M.P., 2015. Neuroinflammation in Alzheimer's disease. The Lancet. Neurology 14 (4), 388–405. https://doi.org/10.1016/S1474-4422(15)70016-5.

Koistinaho, M., Lin, S., Wu, X., Esterman, M., Koger, D., Hanson, J., Higgs, R., Liu, F., Malkani, S., Bales, K.R., Paul, S.M., 2004. Apolipoprotein E promotes astrocyte colocalization and degradation of deposited amyloid-β peptides. Nat. Med. 10 (7), 719–726. https://doi.org/10.1038/nm1058.

Konstantinidis, E., Dakhel, A., Beretta, C., Erlandsson, A., 2023a. Long-term effects of amyloid-beta deposits in human iPSC-derived astrocytes. Mol. Cell. Neurosci. 125, 103839 https://doi.org/10.1016/j.mcn.2023.103839.

Konstantinidis, E., Portal, B., Mothes, T., Beretta, C., Lindskog, M., Erlandsson, A., 2023b. Intracellular deposits of amyloid-beta influence the ability of human iPSC-derived astrocytes to support neuronal function. J. Neuroinflammation 20 (1), 3. https://doi.org/10.1186/s12974-022-02687-5.

Lindström, V., Gustafsson, G., Sanders, L.H., Howlett, E.H., Sigvardson, J., Kasrayan, A., Ingelsson, M., Bergström, J., Erlandsson, A., 2017. Extensive uptake of α-synuclein oligomers in astrocytes results in sustained intracellular deposits and mitochondrial damage. Mol. Cell. Neurosci. 82, 143–156. https://doi.org/10.1016/j.mcn.2017.04.009.

Lööv, C., Mitchell, C.H., Simonsson, M., Erlandsson, A., 2015. Slow degradation in phagocytic astrocytes can be enhanced by lysosomal acidification. Glia 63 (11), 1997–2009. https://doi.org/10.1002/glia.22873.

Lundin, A., Delsing, L., Clausen, M., Ricchiuto, P., Sanchez, J., Sabirsh, A., Ding, M., Synnergren, J., Zetterberg, H., Brolén, G., Hicks, R., Herland, A., Falk, A., 2018. Human iPS-derived astroglia from a stable neural precursor state show improved functionality compared with conventional astrocytic models. Stem Cell Rep. 10 (3), 1030–1045. https://doi.org/10.1016/j.stemcr.2018.01.021.

MacVicar, B.A., Newman, E.A., 2015. Astrocyte regulation of blood flow in the brain. Cold Spring Harb. Perspect. Biol. 7 (5), a020388 https://doi.org/10.1101/cshperspect.a020388.

McLean, C.A., Cherny, R.A., Fraser, F.W., Fuller, S.J., Smith, M.J., Vbeyreuther, K., Bush, A.I., Masters, C.L., 1999. Soluble pool of Aβ amyloid as a determinant of severity of neurodegeneration in Alzheimer's disease. Ann. Neurol. 46 (6), 860–866. https://doi.org/10.1002/1531-8249(199912)46:6<860::AID-ANA8>3.0.CO;2-M.

Michno, W., Stringer, K.M., Enzlein, T., Passarelli, M.K., Escrig, S., Vitanova, K., Wood, J., Blennow, K., Zetterberg, H., Meibom, A., Hopf, C., Edwards, F.A., Hanrieder, J., 2021. Following spatial Aβ aggregation dynamics in evolving Alzheimer's disease pathology by imaging stable isotope labeling kinetics. Science. Advances 7 (25), eabg4855. https://doi.org/10.1126/sciadv.abg4855.

Morizawa, Y.M., Hirayama, Y., Ohno, N., Shibata, S., Shigetomi, E., Sui, Y., Nabekura, J., Sato, K., Okajima, F., Takebayashi, H., Okano, H., Koizumi, S., 2017. Reactive astrocytes function as phagocytes after brain ischemia via ABCA1-mediated pathway. Nat. Commun. 8 (1), 1 https://doi.org/10.1038/s41467-017-00037-1.

Mothes, T., Portal, B., Konstantinidis, E., Eltom, K., Libard, S., Streubel-Gallasch, L., Ingelsson, M., Rostami, J., Lindskog, M., Erlandsson, A., 2023. Astrocytic uptake of neuronal corpses promotes cell-to-cell spreading of tau pathology. Acta Neuropathol. Commun. 11 (1), 97. https://doi.org/10.1186/s40478-023-01589-8.

Mulica, P., Grünewald, A., Pereira, S.L., 2021. Astrocyte-neuron metabolic crosstalk in neurodegeneration: a mitochondrial perspective. Front. Endocrinol. 12, 668517 https://doi.org/10.3389/fendo.2021.668517.

Nagele, R.G., D'Andrea, M.R., Lee, H., Venkataraman, V., Wang, H.Y., 2003. Astrocytes accumulate A beta 42 and give rise to astrocytic amyloid plaques in Alzheimer disease brains. Brain Res. 971 (2), 197–209. https://doi.org/10.1016/S0006-8993(03)02361-8.

Näslund, J., Haroutunian, V., Mohs, R., Davis, K.L., Davies, P., Greengard, P., Buxbaum, J.D., 2000. Correlation between elevated levels of amyloid beta-peptide in the brain and cognitive decline. JAMA 283 (12), 1571–1577. https://doi.org/10.1001/jama.283.12.1571.

Nielsen, H.M., Mulder, S.D., Beliën, J.A.M., Musters, R.J.P., Eikelenboom, P., Veerhuis, R., 2010. Astrocytic A beta 1-42 uptake is determined by A beta-aggregation state and the presence of amyloid-associated proteins. Glia 58 (10), 1235–1246. https://doi.org/10.1002/GLIA.21004.

Nikitidou, E., Khoonsari, P.E., Shevchenko, G., Ingelsson, M., Kultima, K., Erlandsson, A., 2017. Increased release of apolipoprotein E in extracellular vesicles following amyloid-β protofibril exposure of neuroglial co-cultures. Journal of Alzheimer's Disease: JAD 60 (1), 305–321. https://doi.org/10.3233/JAD-170278.

Nixon, R.A., 2020. The aging lysosome: an essential catalyst for late-onset neurodegenerative diseases. Biochim. Biophys. Acta, Proteins Proteomics 1868 (9), 140443. https://doi.org/10.1016/j.bbapap.2020.140443.

Olabarria, M., Noristani, H.N., Verkhratsky, A., Rodríguez, J.J., 2010. Concomitant astroglial atrophy and astrogliosis in a triple transgenic animal model of Alzheimer's disease. Glia 58 (7), 831–838. https://doi.org/10.1002/glia.20967.

Pannee, J., Portelius, E., Minthon, L., Gobom, J., Andreasson, U., Zetterberg, H., Hansson, O., Blennow, K., 2016. Reference measurement procedure for CSF amyloid beta (Aβ)1-42 and the CSF Aβ1-42/Aβ1-40 ratio—a cross-validation study against amyloid PET. J. Neurochem. 139 (4), 651–658. https://doi.org/10.1111/jnc.13838.

Pike, C.J., Cummings, B.J., Monzavi, R., Cotman, C.W., 1994. Beta-amyloid-induced changes in cultured astrocytes parallel reactive astrocytosis associated with senile plaques in Alzheimer's disease. Neuroscience 63 (2), 517–531. https://doi.org/10.1016/0306-4522(94)90547-9.

Rostami, J., Holmqvist, S., Lindström, V., Sigvardson, J., Westermark, G.T., Ingelsson, M., Bergström, J., Roybon, L., Erlandsson, A., 2017. Human astrocytes transfer aggregated alpha-synuclein via tunneling nanotubes. J. Neurosci. 37 (49), 11835–11853. https://doi.org/10.1523/JNEUROSCI.0983-17.2017.

Rostami, J., Mothes, T., Kolahdouzan, M., Eriksson, O., Moslem, M., Bergström, J., Ingelsson, M., O'Callaghan, P., Healy, L.M., Falk, A., Erlandsson, A., 2021. Crosstalk between astrocytes and microglia results in increased degradation of α-synuclein and amyloid-β aggregates. J. Neuroinflammation 18 (1), 124. https://doi.org/10.1186/s12974-021-02158-3.

Serrano-Pozo, A., Frosch, M.P., Masliah, E., Hyman, B.T., 2011. Neuropathological alterations in Alzheimer disease. Cold Spring Harb. Perspect. Med. 1 (1), a006189 https://doi.org/10.1101/cshperspect.a006189.

Söllvander, S., Nikitidou, E., Brolin, R., Söderberg, L., Sehlin, D., Lannfelt, L., Erlandsson, A., 2016. Accumulation of amyloid-β by astrocytes result in enlarged endosomes and microvesicle-induced apoptosis of neurons. Mol. Neurodegener. 11 (1), 38. https://doi.org/10.1186/s13024-016-0098-z.

Streubel-Gallasch, L., Giusti, V., Sandre, M., Tessari, I., Plotegher, N., Giusto, E., Masato, A., Iovino, L., Battisti, I., Arrigoni, G., Shimshek, D., Greggio, E., Tremblay, M.-E., Bubacco, L., Erlandsson, A., Civiero, L., 2021. Parkinson's disease-associated LRRK2 interferes with astrocyte-mediated alpha-synuclein clearance. Mol. Neurobiol. 58 (7), 3119–3140. https://doi.org/10.1007/s12035-021-02327-8.

Thal, D.R., Schultz, C., Dehghani, F., Yamaguchi, H., Braak, H., Braak, E., 2000. Amyloid beta-protein (Abeta)-containing astrocytes are located preferentially near N-terminal-truncated Abeta deposits in the human entorhinal cortex. Acta Neuropathol. 100 (6), 608–617. https://doi.org/10.1007/s004010000242.

Vasile, F., Dossi, E., Rouach, N., 2017. Human astrocytes: structure and functions in the healthy brain. Brain Struct. Funct. 222 (5), 2017–2029. https://doi.org/10.1007/s00429-017-1383-5.

Verkhratsky, A., Matteoli, M., Parpura, V., Mothet, J.-P., Zorec, R., 2016. Astrocytes as secretory cells of the central nervous system: idiosyncrasies of vesicular secretion. EMBO J. 35 (3), 239–257. https://doi.org/10.15252/embj.201592705.

Wildburger, N.C., Esparza, T.J., LeDuc, R.D., Fellers, R.T., Thomas, P.M., Cairns, N.J., Kelleher, N.L., Bateman, R.J., Brody, D.L., 2017. Diversity of amyloid-beta proteoforms in the Alzheimer's disease brain. Sci. Rep. 7 (1), 1 https://doi.org/10.1038/s41598-017-10422-x.

Zyśk, M., Beretta, C., Naia, L., Dakhel, A., Påvénius, L., Brismar, H., Lindskog, M., Ankarcrona, M., Erlandsson, A., 2023. Amyloid-β accumulation in human astrocytes induces mitochondrial disruption and changed energy metabolism. J. Neuroinflammation 20 (1), 43. https://doi.org/10.1186/s12974-023-02722-z.